Unlocking the Potential of Cation-Disordered Oxides for Rechargeable Lithium Batteries

Jinhyuk Lee *et al.*

Science **343**, 519 (2014);
DOI: 10.1126/science.1246432

order modes to circumvent this issue. We envision that this concept may open new directions in acoustics research, including advances in noise control, transducer technologies, energy harvesting systems, acoustic imaging, and sensing.

References and Notes

1. H. B. G. Casimir, *Rev. Mod. Phys.* **17**, 343–350 (1945).
2. Z. Wang, S. Fan, *Appl. Phys. B* **81**, 369–375 (2005).
3. Z. Yu, S. Fan, *Nat. Photonics* **3**, 91–94 (2009).
4. L. Bi *et al.*, *Nat. Photonics* **5**, 758–762 (2011).
5. A. Kamal, J. Clarke, M. H. Devoret, *Nat. Phys.* **7**, 311–315 (2011).
6. T. Kodera, D. L. Sounas, C. Caloz, *Appl. Phys. Lett.* **99**, 031114, 031114–3 (2011).
7. M. S. Kang, A. Butsch, P. S. J. Russell, *Nat. Photonics* **5**, 549–553 (2011).
8. D.-W. Wang *et al.*, *Phys. Rev. Lett.* **110**, 093901 (2013).
9. H. Lira, Z. Yu, S. Fan, M. Lipson, *Phys. Rev. Lett.* **109**, 033901 (2012).
10. D. L. Sounas, C. Caloz, A. Alù, *Nat. Commun.* **4**, 2407 (2013).
11. S. Lepri, G. Casati, *Phys. Rev. Lett.* **106**, 164101 (2011).
12. M. Soljačić, C. Luo, J. D. Joannopoulos, S. Fan, *Opt. Lett.* **28**, 637–639 (2003).
13. I. V. Shadrivov, V. A. Fedotov, D. A. Powell, Y. S. Kivshar, N. I. Zheludev, *New J. Phys.* **13**, 033025 (2011).
14. L. Fan *et al.*, *Science* **335**, 447–450 (2012).
15. B. Liang, B. Yuan, J. C. Cheng, *Phys. Rev. Lett.* **103**, 104301 (2009).
16. B. Liang, X. S. Guo, J. Tu, D. Zhang, J. C. Cheng, *Nat. Mater.* **9**, 989–992 (2010).
17. N. Boechler, G. Theocharis, C. Daraio, *Nat. Mater.* **10**, 665–668 (2011).
18. X.-F. Li *et al.*, *Phys. Rev. Lett.* **106**, 084301 (2011).
19. X. Zhu, X. Zou, B. Liang, J. Cheng, *J. Appl. Phys.* **108**, 124909, 124909–5 (2010).
20. Z. He *et al.*, *Appl. Phys. Lett.* **98**, 083505, 083505–3 (2011).
21. H. Sun, S. Zhang, X. Shui, *Appl. Phys. Lett.* **100**, 103507, 103507–4 (2012).
22. A. Cicek, O. Adem Kaya, B. Ulug, *Appl. Phys. Lett.* **100**, 111905, 111905–4 (2012).
23. J. Hwan Oh, H. Woong Kim, P. Sik Ma, H. Min Seung, Y. Young Kim, *Appl. Phys. Lett.* **100**, 213503, 213503–213504 (2012).
24. B. Yuan, B. Liang, J. Tao, X. Zou, J. Cheng, *Appl. Phys. Lett.* **101**, 043503, 043503–043504 (2012).
25. D. Jalas *et al.*, *Nat. Photonics* **7**, 579–582 (2013).
26. A. A. Maznev, A. G. Every, O. B. Wright, *Wave Motion* **50**, 776–784 (2013).
27. C. Kittel, *Phys. Rev.* **110**, 836–841 (1958).
28. L. M. Brekhovskikh, I. P. Lysanov, *Fundamentals of Ocean Acoustics* (Springer, Berlin, 2003).
29. C. Cohen-Tannoudji, B. Diu, F. Laloë, *Quantum Mechanics*, vol. 1 (Hermann, Wiley, NY, 1991).
30. Materials and methods are available as supplemenatry materials on *Science* Online.

Acknowledgments: This work has been supported by the Defense Threat Reduction Agency Young Investigator Program (YIP) award HDTRA1-12 1-0022 and the Air Force Office of Scientific Research YIP award FA9550-11-1-0009. A provisional U.S. patent has been filed with title "Non-reciprocal acoustic devices based on angular momentum bias" (61/868,178). R.F., D.L.S., and A.A. developed the concept presented in this paper. R.F. and D.L.S. carried out the analytical and numerical modeling and built the device. R.F. and C.F.S. conducted the measurements. M.R.H. contributed to the design and realization of the experimental set-up. A.A. supervised the entire project. All authors discussed the results and commented on the article.

Supplementary Materials

www.sciencemag.org/content/343/6170/516/suppl/DC1
Materials and Methods
Fig. S1
References (*31*–*35*)

8 October 2013; accepted 3 December 2013
10.1126/science.1246957

Unlocking the Potential of Cation-Disordered Oxides for Rechargeable Lithium Batteries

Jinhyuk Lee,[1] Alexander Urban,[1]* Xin Li,[1]* Dong Su,[2] Geoffroy Hautier,[1] Gerbrand Ceder[1]†

Nearly all high–energy density cathodes for rechargeable lithium batteries are well-ordered materials in which lithium and other cations occupy distinct sites. Cation-disordered materials are generally disregarded as cathodes because lithium diffusion tends to be limited by their structures. The performance of $Li_{1.211}Mo_{0.467}Cr_{0.3}O_2$ shows that lithium diffusion can be facile in disordered materials. Using ab initio computations, we demonstrate that this unexpected behavior is due to percolation of a certain type of active diffusion channels in disordered Li-excess materials. A unified understanding of high performance in both layered and Li-excess materials may enable the design of disordered-electrode materials with high capacity and high energy density.

Rechargeable lithium-ion batteries enable increasingly capable portable electronics and are the crucial factor in the deployment of electric vehicles. Cathodes with high energy density are desirable for high-performance lithium batteries, as they make up a substantial part of the cost, weight, and volume of a battery. Cathode compounds operate by reversibly releasing (de-intercalation) and reinserting (intercalation) lithium ions during charge and discharge, respectively. This process must occur without causing permanent change to the crystal structure because the battery must endure hundreds of charge-discharge cycles. Traditionally, cathodes have been sought from well-ordered close-packed oxides—in particular, layered rocksalt-type lithium–transition metal oxides (Li-TM oxides) (*1*–*3*) and ordered spinels (*4*, *5*)—whereas nonordered materials have received limited attention (*6*–*9*). In these ordered compounds, Li sites and pathways (a 2D slab in the layered oxides and a 3D network of tetrahedral sites in the spinels) are separated from the TM sublattice, which provides stability and electron storage capacity. Having well-ordered structures where there is little or no intermixing between the Li and the TM sublattice is generally considered important for obtaining high-capacity cathode materials with good cycle life (*10*, *11*). In some cases, improvements in ordering have led to notable increases in power or energy density (*3*, *12*–*14*). Here, we show that this "ordering paradigm" may have led the community to overlook a large class of cathode materials in which Li and TM share the same sublattice in a random (disordered) fashion; some of these materials may offer higher capacity and better stability relative to the layered oxides.

[1]Department of Materials Science and Engineering, Massachusetts Institute of Technology, Cambridge, MA 02139, USA. [2]Center for Functional Nanomaterials, Brookhaven National Laboratory, Upton, NY 11973, USA.

*These authors contributed equally to this work.
†Corresponding author. E-mail: gceder@mit.edu

We chose the $Li_{1.211}Mo_{0.467}Cr_{0.3}O_2$ (LMCO) compound because of our interest in metals that can exchange multiple electrons, such as Mo and Cr. In addition, both Mo and Cr have been shown to migrate in layered materials (*15*, *16*). LMCO was synthesized through standard solid-state procedures as described (*17*). The material forms as a layered rocksalt but transforms to a disordered rocksalt after just a few charge-discharge cycles, as seen in the x-ray diffraction (XRD) patterns in Fig. 1A. The (003) reflection, characteristic of the layered structure, starts to disappear after one cycle and is essentially gone at the 10th cycle. From Rietveld refinement, we estimate 34 to 52% of the TM ions to be in Li layers after 10 cycles, indicating substantial cation mixing in LMCO (*17*). The evolution of LMCO to a disordered structure was confirmed in real space with scanning transmission electron microscopy (STEM) (Fig. 1B). The bright and dark columns in the "before" image correspond to atomic columns of mixed Li-Mo-Cr ions and Li ions, respectively. The Z-contrast decreases after one cycle and is very weak after 10 cycles, indicating increased cation mixing. This substantial structural evolution is consistent with the change in voltage profile (Fig. 1C) between the first charge and all subsequent cycles.

The reversible Li capacity of carbon-coated LMCO (LMCO/C) is remarkably high, even after disordering (*17*). As seen in Fig. 1C, approximately one lithium (= 265.6 mAh g^{-1}) per formula unit can be reversibly cycled at C/20 rate [= 16.4 mA g^{-1}; the C/*n* rate denotes the rate of cycling the theoretical capacity of LMCO (327.5 mAh g^{-1}) in *n* hours], delivering an energy density of ~660 Wh/kg (~3100 Wh/liter) at ~2.5 V. Such high capacity is rarely achieved even in layered Li-TM oxides (*18*–*20*) and is counter-intuitive because cation mixing has been argued to markedly degrade the cyclability of layered oxides, primarily by reducing the Li layer spacing

(Li slab distance), resulting in limited Li diffusion (*3*, *12*, *14*, *21*–*24*). Indeed, given that the oxygen-interlayer (slab) distance around the Li layer of LMCO decreases considerably from ~2.63 Å to ~2.39 Å after disordering (*17*), negligible Li mobility would be expected (*3*, *14*, *23*).

In a disordered rocksalt, both Li and TM occupy a cubic close-packed lattice of octahedral sites, and Li diffusion proceeds by hopping from one octahedral site to another octahedral site via an intermediate tetrahedral site (*o-t-o* diffusion; Fig. 2A) (*17*, *23*, *25*). Li in the intermediate tetrahedral site is the activated state in Li diffusion. The activated tetrahedral Li^+ ion shares faces with four octahedral sites: the site previously occupied by the ion itself; the vacancy it will move into; and two sites that can be occupied by Li, TM, or a vacancy. The energy in this state, which reflects the Li migration barrier, is largely determined by electrostatic repulsion between the activated Li^+ ion and its face-sharing species, and thus depends on (i) the valence of the face-sharing species and (ii) the available space for relaxation between the activated Li^+ ion and the face-sharing species. This space is measurable as the Li slab distance in layered structures (*3*, *14*, *23*), or more generally as the height of the tetrahedron along which the relaxation occurs (Fig. 2A).

As electrostatic repulsion on an activated Li^+ ion is too strong when there are two face-sharing cations, Li dominantly diffuses with the divacancy mechanism, involving a second vacancy beside the vacancy the migrating Li will move into (*3*, *23*, *25*). In rocksalt-type Li-TM oxides, two kinds of diffusion channels support this mechanism: 0-TM channels, involving no face-sharing TM ion (Fig. 2B), and 1-TM channels, involving one face-sharing TM ion (Fig. 2C). Note that 1-TM channels are responsible for Li diffusion in typical layered Li-TM oxides. To investigate which channels in disordered LMCO allow for reasonable hopping rates, we calculated Li migration barriers for 1-TM and 0-TM channels using density functional theory (DFT), according to the divacancy mechanism (*17*).

The red and blue dashed lines in Fig. 3 show the mean migration barriers along a 1-TM channel as a function of the average tetrahedron height of model disordered structures (disordered Li_2MoO_3, disordered $LiCrO_2$) when the face-sharing octahedral species is Mo^{4+} and Cr^{3+}, respectively (*17*). Note that migration barriers in disordered structures vary with the local atomic environment, which accounts for a distribution of migration barriers. The mean barrier increases as the tetrahedron height (h) decreases, reaching ~510 meV along a 1-Mo^{4+} channel and ~490 meV along a 1-Cr^{3+} channel at h ~ 2.39 Å, the average tetrahedron height in disordered LMCO (*17*). Note that these barriers tend to increase as the transition metal becomes oxidized in charge. Considering that typical 1-TM barriers in layered oxides are ~300 meV (*23*), such high barriers in disordered LMCO indicate very limited Li diffusion along 1-TM channels. This is because the small tetrahedron height in disordered LMCO confines the activated Li^+ ion close to a face-sharing high-valent octahedral TM ion in 1-TM channels, resulting in strong electrostatic repulsion on the Li^+ ion.

The black dashed line in Fig. 3 shows the mean migration barriers along 0-TM channels. In contrast to the high barriers in 1-TM channels, the low barrier at h ~ 2.39 Å (~290 meV) indicates that Li migration along 0-TM channels will still be facile in disordered LMCO, with a hopping rate higher than that along 1-TM channels by a factor of ~4400 [exp(−290 meV/kT)/exp(−500 meV/kT)] at room temperature. The low valence of a face-

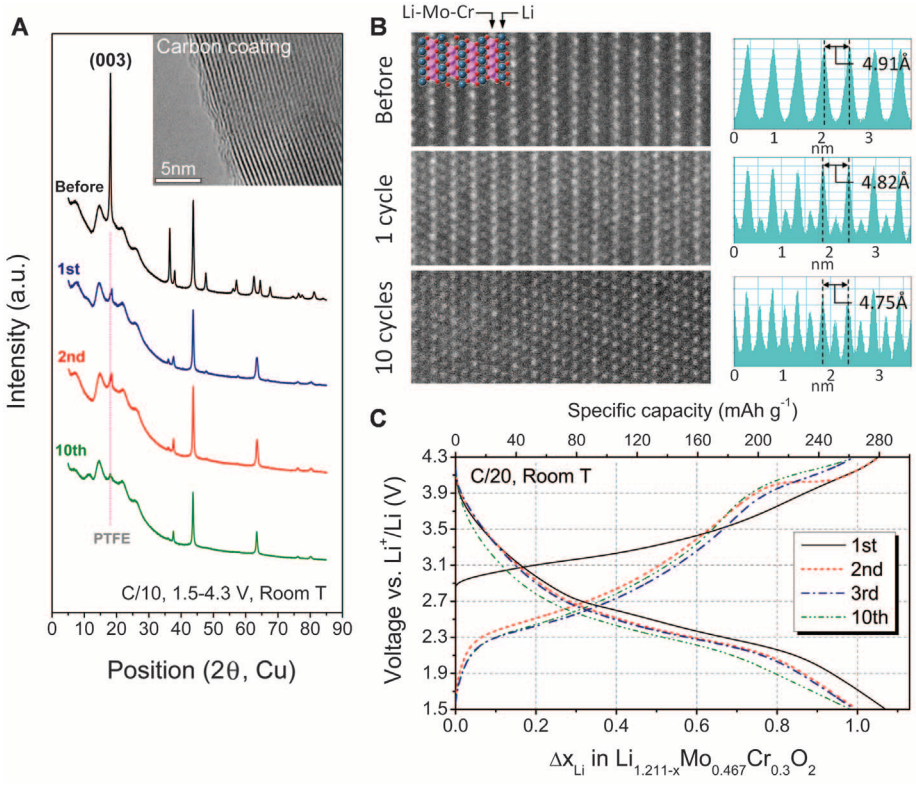

Fig. 1. $Li_{1.211}Mo_{0.467}Cr_{0.3}O_2$ shows high Li cycling capacity even after substantial cation disordering. (**A**) XRD patterns of C-coated $Li_{1.211}Mo_{0.467}Cr_{0.3}O_2$ (LMCO/C) electrodes before and after 1, 2, and 10 cycles, 1.5 to 4.3 V, C/10. The inset image shows the C-coating layer. (**B**) Left: STEM images along the [010] zone axis in a LMCO/C particle before cycling and after 1 and 10 cycles, 1.5 to 4.3 V, C/20. Right: Corresponding line profiles of the Z-contrast information with the measured spacing of Li-Mo-Cr layers. (**C**) Voltage profile of LMCO/C, 1.5 to 4.3 V, C/20.

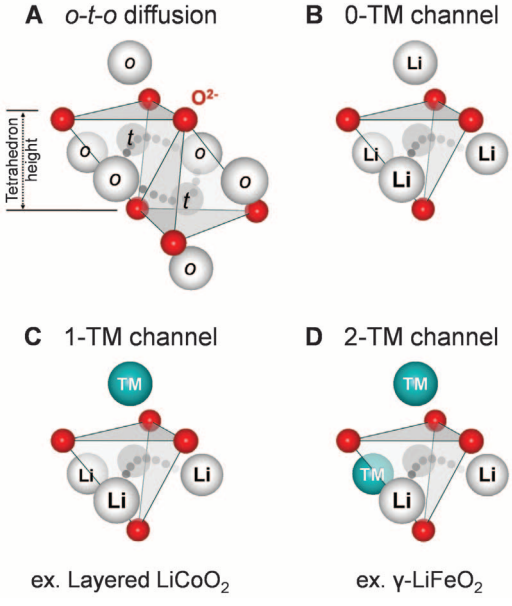

Fig. 2. Possible environments for an *o-t-o* Li hop in rocksalt-like Li-TM oxides. (**A**) *o-t-o* diffusion: Two tetrahedral paths connect each pair of neighboring octahedral sites. (**B** to **D**) The activated state can share faces with no octahedral transition metals (0-TM channel) (B), one transition metal (1-TM channel) (C), or two transition metals (2-TM channel) (D).

sharing octahedral Li^+ ion (versus Mo^{4+} or Cr^{3+}) results in much weaker electrostatic repulsion on the activated Li^+ ion in 0-TM channels. At highly charged states, tetrahedral Li may form in some 0-TM channels because high delithiation should leave no face-sharing octahedral Li at all (*26*). However, the mean migration barrier between two 0-TM tetrahedral sites was calculated to be ~415 meV, indicating that Li can easily escape from these sites.

Herein lies the real issue of (cation) disordered structures: 1-TM channels, which account for the excellent Li mobility in the layered intercalation oxides that currently dominate the battery industry, become nearly inactive in disordered materials as a result of their small tetrahedron heights. In contrast, 0-TM channels are active in disordered rocksalts but are much less frequent than 1-TM channels. Nonetheless, as we show below, 0-TM channels start to enable facile macroscopic diffusion in disordered structures once enough Li excess is introduced.

For 0-TM channels to dominate macroscopic Li diffusion, they must be continuously connected through the entire material, forming a percolating network uninterrupted by 1-TM and 2-TM channels. To establish a general understanding of 0-TM percolation, we studied (i) when 0-TM channels percolate in a rocksalt-type Li-TM oxide and (ii) which fraction of the Li ions become part of a percolating network of 0-TM channels.

Figure 4A shows the probability of finding a percolating network of 0-TM channels (0-TM network) in a rocksalt-type Li-TM oxide as a function of Li content (x in $Li_xTM_{2-x}O_2$) and cation mixing ($TM_{Li\ layers}/TM_{TM\ layers} \times 100\%$), as obtained by Monte Carlo simulations (*17*). The probability (color-coded) steeply increases from 0 (red) to 1 (blue) across the black line in Fig. 4A (percolation threshold), varying from x ~ 1.13 for layered oxides to x ~ 1.09 for fully disordered oxides. Because 0-TM channels require a locally Li-rich environment, excess Li ($x \geq$ ~1.09) is essential to open the percolating 0-TM network.

To estimate the contribution of a percolating 0-TM network to macroscopic Li diffusion, we investigated how Li excess and cation mixing affect the Li content in the network (Fig. 4B), which we refer to as accessible Li. This Li can diffuse through the network without traversing 1-TM or 2-TM channels, whereas "inaccessible" Li must traverse 1-TM or 2-TM channels to reach the percolating 0-TM network. The three black lines in Fig. 4B are the contour lines where the accessible Li content is 0.8 Li, 1 Li, and 1.2 Li per $Li_xTM_{2-x}O_2$. For $x \leq 1$, no percolating 0-TM network exists (Fig. 4A) and hence there is no accessible Li content, which explains why stoichiometric $LiTMO_2$ compounds have low capacity when cation-disordered (*7*, *9*, *21*, *24*). However, the accessible Li content gradually increases as x exceeds ~1.09 (percolation threshold), and becomes as high as 1 Li as x exceeds ~1.22 regardless of cation mixing. Increasing Li excess adds more 0-TM channels to a percolating 0-TM network, improving the network's connectivity.

The above results explain how Li diffusion can be facile in disordered LMCO. LMCO is a Li-excess material with $x = 1.233$ in $Li_xTM_{2-x}O_2$. With this Li content, 0-TM channels will be percolating (Fig. 4A), accessing as high as ~1 Li per formula unit (Fig. 4B). Therefore, even as 1-TM channels become nearly inactive after disordering (Fig. 3), a large fraction of Li in the material can still be cycled through the percolating active 0-TM network.

The principle of creating a percolating 0-TM network can be applied to the design of other high-performing disordered Li-TM oxides for two reasons. First, the 0-TM activated state is surrounded only by Li sites, making the effect of the TM species on the activation energy less pronounced. Second, as shown in table S1 (*17*), the tetrahedron height of most disordered rocksalts is such that 0-TM channels are calculated to be active (Fig. 3). Therefore, a percolating 0-TM network will likely enable facile Li diffusion in other disordered materials, assuming that no other kinetic barriers become limiting. Note that the few cation-disordered materials in the literature that were electrochemically active are indeed Li-excess materials, whereas stoichiometric disordered materials are usually not electrochemically active, which is consistent with our understanding (*7*–*9*, *16*, *21*, *24*).

Disordered Li-excess rocksalts have considerable advantages over layered materials. We find that the changes in lattice parameters and volume, as a function of Li concentration, are very small in disordered materials (<1% in LMCO), which will lead to less mechanical stress and capacity loss in an electrode (fig. S8). Furthermore, as they have more homogeneous cation distribution, they tend to experience less change in local environment

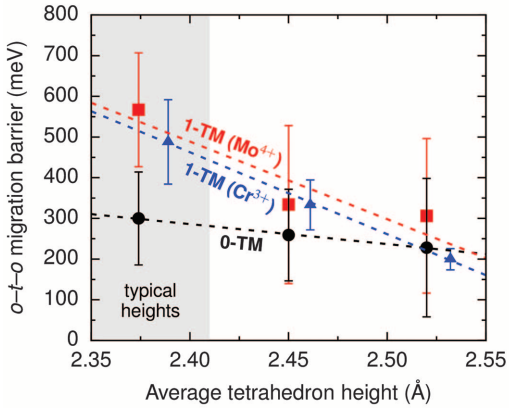

Fig. 3. Li hopping through 0-TM channels can still be facile in cation-disordered materials. Calculated Li migration barriers along 1-TM (Mo^{4+}) channels (red squares), 1-TM (Cr^{3+}) channels (blue triangles), and 0-TM (Li^+) channels (black circles) as a function of the average tetrahedron height of model disordered structures (disordered Li_2MoO_3, disordered $LiCrO_2$). Error bars denote SD. The shaded area highlights typical tetrahedron heights of disordered materials (*17*).

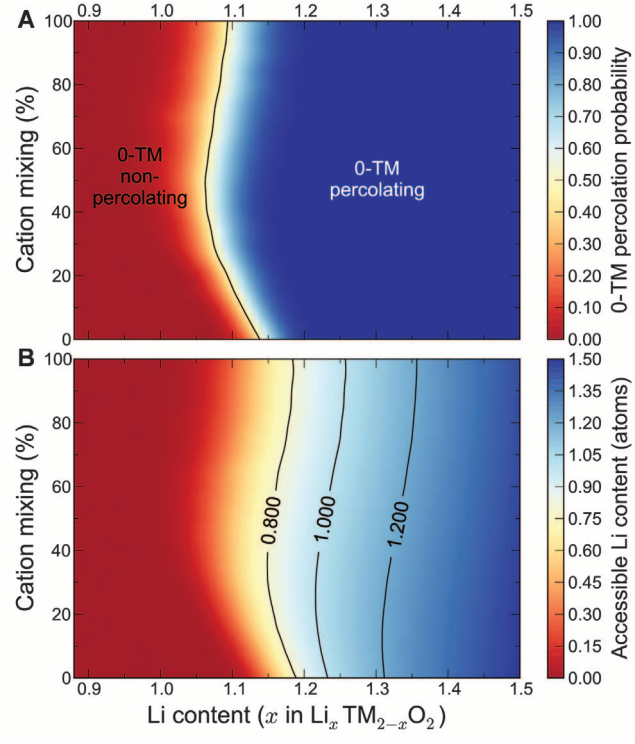

Fig. 4. Li excess opens a percolating network of 0-TM channels in rocksalt-type Li-TM oxides. (**A**) Computed probability of finding a percolating network of 0-TM channels (color) versus Li content (x in $Li_xTM_{2-x}O_2$) and cation mixing ($TM_{Li\ layers}/TM_{TM\ layers} \times 100\%$). (**B**) Accessible Li content by a percolating 0-TM network (color) versus Li content and cation mixing. In the simulation, cations were randomly distributed at each cation-mixing level (*17*).

of the lithium ions as a function of state of charge. This change in environment is particularly problematic in layered structures where the slab spacing decreases considerably when large amounts of Li are removed, leading to a substantial reduction of Li mobility (*25*, *27*, *28*). However, in cation-disordered structures, homogeneously distributed cations should lead to a Li diffusivity that is more independent of the Li concentration, as is the case for electrode materials with the spinel- and olivine-type structures. One issue that requires more investigation is whether cation disordering will lead to a more sloped voltage profile than for well-ordered materials, as one would expect from the wider distribution of Li-site energies in a disordered material. However, this variance in the Li-site energy may be counteracted by a less effective Li-Li interaction, which is responsible for the slope of the voltage curve in layered materials (*29*). Hence, careful tailoring of the TM-Li to Li-Li ion interaction may mitigate this effect. Given the insights presented above, it may not be surprising that the highest-capacity layered materials are highly Li-excess materials (*18*–*20*) that become more disordered in the first few cycles because of a particular overcharge mechanism (*30*).

Our results may explain why disorder has not been pursued as a strategy before: Most materials synthesized are near stoichiometry ($LiTMO_2$), which is well below the percolation threshold for 0-TM diffusion. Therefore, these materials quickly lose their capacity upon disorder as it renders typical 1-TM channels inactive, while 0-TM channels are not percolating (*7*, *9*, *21*, *24*). As a result, disorder may have appeared to be a counter-intuitive strategy. In contrast, our analysis points to cation-disordered materials as a class of materials that can exhibit high capacity and high energy density, thereby offering hope for substantial improvements in the performance of rechargeable Li batteries.

References and Notes

1. K. Mizushima, P. C. Jones, P. J. Wiseman, J. B. Goodenough, *Mater. Res. Bull.* **15**, 783–789 (1980).
2. T. Ohzuku, A. Ueda, M. Nagayama, *J. Electrochem. Soc.* **140**, 1862–1870 (1993).
3. K. Kang, Y. S. Meng, J. Bréger, C. P. Grey, G. Ceder, *Science* **311**, 977–980 (2006).
4. M. M. Thackeray, P. J. Johnson, L. A. De Picciotto, P. G. Bruce, J. B. Goodenough, *Mater. Res. Bull.* **19**, 179–187 (1984).
5. K. M. Shaju, P. G. Bruce, *Dalton Trans.* **2008**, 5471–5475 (2008).
6. A. J. Jacobson, R. R. Chianelli, S. M. Rich, M. S. Whittingham, *Mater. Res. Bull.* **14**, 1437–1448 (1979).
7. M. N. Obrovac, O. Mao, J. R. Dahn, *Solid State Ion.* **112**, 9–19 (1998).
8. V. Pralong, V. Gopal, V. Caignaert, V. Duffort, B. Raveau, *Chem. Mater.* **24**, 12–14 (2012).
9. Y. Sakui, H. Arai, J.-i. Yamaki, *Solid State Ion.* **113-115**, 29–34 (1998).
10. M. S. Whittingham, *Chem. Rev.* **104**, 4271–4302 (2004).
11. J. B. Goodenough, Y. Kim, *Chem. Mater.* **22**, 587–603 (2010).
12. A. Rougier, I. Saadoune, P. Gravereau, P. Willmann, C. Delmas, *Solid State Ion.* **90**, 83–90 (1996).
13. Z. Lu, D. D. MacNeil, J. R. Dahn, *Electrochem. Solid State Lett.* **4**, A200–A203 (2001).
14. A. Rougier, P. Gravereau, C. Delmas, *J. Electrochem. Soc.* **143**, 1168–1175 (1996).
15. A. C. W. P. James, J. B. Goodenough, *J. Solid State Chem.* **76**, 87–96 (1988).
16. L. Zhang, H. Noguchi, *J. Electrochem. Soc.* **150**, A601–A607 (2003).
17. See supplementary materials on *Science* Online.
18. C. S. Johnson *et al.*, *Electrochem. Commun.* **6**, 1085–1091 (2004).
19. M. Sathiya *et al.*, *Nat. Mater.* **12**, 827–835 (2013).
20. Z. Lu, J. R. Dahn, *J. Electrochem. Soc.* **149**, A815–A822 (2002).
21. K. Kang *et al.*, *Chem. Mater.* **15**, 4503–4507 (2003).
22. J. Peres *et al.*, *J. Phys. Chem. Solids* **57**, 1057–1060 (1996).
23. K. Kang, G. Ceder, *Phys. Rev. B* **74**, 094105 (2006).
24. K. Ozawa *et al.*, *J. Power Sources* **174**, 469–472 (2007).
25. A. Van der Ven, G. Ceder, *Electrochem. Solid State Lett.* **3**, 301–304 (2000).
26. J. Bréger *et al.*, *Chem. Mater.* **18**, 4768–4781 (2006).
27. A. Van der Ven, M. K. Aydinol, G. Ceder, G. Kresse, J. Hafner, *Phys. Rev. B* **58**, 2975–2987 (1998).
28. G. G. Amatucci, J. M. Tarascon, L. C. Klein, *J. Electrochem. Soc.* **143**, 1114–1123 (1996).
29. A. Van der Ven, M. K. Aydinol, G. Ceder, *J. Electrochem. Soc.* **145**, 2149–2155 (1998).
30. N. Yabuuchi, K. Yoshii, S. T. Myung, I. Nakai, S. Komaba, *J. Am. Chem. Soc.* **133**, 4404–4419 (2011).

Acknowledgments: Supported by the Robert Bosch Corporation, by Umicore Specialty Oxides and Chemicals, and by a Samsung Scholarship (J.L.). Computational resources from the National Energy Research Scientific Computing Center (NERSC) and from the Extreme Science and Engineering Discovery Environment (XSEDE) are gratefully acknowledged. The STEM work carried out at the Center for Functional Nanomaterials, Brookhaven National Laboratory, was supported by the U.S. Department of Energy, Office of Basic Energy Sciences, under contract DE-AC02-98CH10886. We thank N. Twu, S. Kim, and J. Kim for valuable discussions.

Supplementary Materials

www.sciencemag.org/content/343/6170/519/suppl/DC1
Materials and Methods
Supplementary Text
Figs. S1 to S8
Table S1
References (*31*–*46*)

25 September 2013; accepted 24 December 2013
Published online 9 January 2014;
10.1126/science.1246432

Low Core-Mantle Boundary Temperature Inferred from the Solidus of Pyrolite

Ryuichi Nomura,[1]* Kei Hirose,[1,2,3]* Kentaro Uesugi,[4] Yasuo Ohishi,[4] Akira Tsuchiyama,[5] Akira Miyake,[5] Yuichiro Ueno[1,2]

The melting temperature of Earth's mantle provides key constraints on the thermal structures of both the mantle and the core. Through high-pressure experiments and three-dimensional x-ray microtomographic imaging, we showed that the solidus temperature of a primitive (pyrolitic) mantle is as low as 3570 ± 200 kelvin at pressures expected near the boundary between the mantle and the outer core. Because the lowermost mantle is not globally molten, this provides an upper bound of the temperature at the core-mantle boundary (T_{CMB}). Such remarkably low T_{CMB} implies that the post-perovskite phase is present in wide areas of the lowermost mantle. The low T_{CMB} also requires that the melting temperature of the outer core is depressed largely by impurities such as hydrogen.

The core-mantle boundary (CMB), located at a depth of 2900 km inside Earth, is the interface between molten metal and rock. The temperature jump across the thermal boundary layer (TBL) above the CMB has been believed to be about 1500 K (*1*), which has important consequences for the dynamics and thermal evolution in the mantle and the core. The temperature at the top of the core should be lower than the solidus temperature of a primitive mantle to avoid global melting above the CMB. Conventionally, the temperature at the CMB (T_{CMB}) has been estimated to be about 4000 K, primarily based on the melting temperature of iron at the inner core boundary (ICB), where solid and liquid cores coexist (*1*–*3*). Such high T_{CMB} implies that $MgSiO_3$-rich post-perovskite, a primary mineral in the lowermost mantle, changes back into perovskite with steeply increasing temperature near the CMB (*4*), which allows detailed modeling of the thermal structure in the CMB region and the heat flux from the core into the mantle (*5*). Previous experiments using laser-heated diamond-anvil cell (DAC) techniques showed that the solidus temperature of a primitive mantle is about 4200 K at the CMB, supporting the high T_{CMB} around 4000 K (*6*–*8*). The

[1]Department of Earth and Planetary Sciences, Tokyo Institute of Technology, Meguro, Tokyo 152-8551, Japan. [2]Earth-Life Science Institute, Tokyo Institute of Technology, Meguro, Tokyo 152-8551, Japan. [3]Institute for Research on Earth Evolution, Japan Agency for Marine-Earth Science and Technology, Yokosuka, Kanagawa 237-0061, Japan. [4]Japan Synchrotron Radiation Research Institute, Sayo, Hyogo 679-5198, Japan. [5]Division of Earth and Planetary Sciences, Kyoto University, Kyoto, Kyoto 606-8502, Japan.

*Corresponding author. E-mail: nomura.r.ab@m.titech.ac.jp (R.N.); kei@elsi.jp (K.H.)